J. Webster (ed.), *Wiley Encyclopedia of Electrical and Electronics Engineering*
Copyright © 1999 John Wiley & Sons, Inc.

INDUCTION MOTOR DRIVES

The cage-rotor induction motor is extremely robust and reliable and requires minimal maintenance. When operating on the normal utility ac supply, the motor speed is essentially constant, and for fixed-speed applications, the cage-rotor induction motor has become the industry workhorse. For applications requiring control of torque, speed or position, the dc motor has traditionally been used because of its easy controllability; however, the commutator imposes inspection and maintenance requirements and restricts motor speed and power ratings. Thus, the induction motor is a desirable alternative to the dc motor in many applications but its control is much more complex. However, modern developments in power electronics and microelectronics have endowed induction motor drives with the sophisticated control and intelligence to equal or surpass the performance of dc motor drives in the most demanding applications. Induction motors are now found in many diverse areas; they drive paper machines, textile machines, conveyors, machine tools, robots, locomotives, automobiles, and so on.

Induction Motors

In the induction motor, the stationary member or *stator,* and the inner rotating member or *rotor,* are separated by a short air gap. Both stator and rotor are fitted with windings that carry alternating currents. The alternating current (*ac*) is supplied directly to the stator winding, and by *induction* (transformer action) to the rotor winding—hence the name induction motor.

The three-phase stator winding consists of three identical groups or phases, which are symmetrically placed, 120° apart, in slots on the inner surface of the stator. The conductors for each phase are spread over a number of adjacent slots to give a *distributed* winding, which establishes an approximately sinusoidal distribution of magnetic flux density around the air-gap periphery. When the stator winding is energized by a three-phase ac supply, the phase currents are displaced in time by one-third of a cycle and vary sinusoidally. The resulting flux density wave in the air-gap has a sinusoidal spatial distribution and rotates at a constant angular velocity, determined by the angular frequency ω_e of the stator currents. In general, if the stator is wound for p pairs of poles, the speed of rotation of the flux wave is $\omega_s = \omega_e/p$ rad/s or $n_s = 60f_e/p$ rpm, where f_e is the supply frequency in hertz (Hz). This is the *synchronous speed* of the induction motor.

The most common type of induction motor has a *cage rotor* (or *squirrel cage rotor*) in which uninsulated aluminum or copper bars are placed in slots on the outer surface of the rotor. These conductors are short-circuited at each end by conducting end-rings, giving a robust, inexpensive and brushless machine. In the less popular *wound rotor* induction motor, the rotor winding has the same distributed three-phase form as the stator winding and its three terminals are connected to three slip-rings. External electrical connection can be made to the rotor winding via stationary carbon brushes bearing on the rotating slip rings; however, for normal operation, the rotor winding is short-circuited by connecting together the three brushes.

Torque Production. As the rotating flux wave produced by the stator currents sweeps past the rotor conductors, it generates an emf in them which causes current to flow in the shorted rotor winding. These

induced rotor currents interact with the air-gap field to produce a torque that causes the rotor to rotate in the same direction as the rotating field. Because of the low resistance of the shorted rotor winding, only a small relative speed difference between the rotating flux wave and the rotor winding is required to produce the necessary rotor emf and current. Consequently, the rotor typically rotates at a speed n rpm, which is only slightly less than the synchronous speed n_s. The fractional slip s is defined as the relative speed difference (n_s-n), expressed as a fraction of the synchronous speed n_s. Thus, $s = (n_s\text{-}n)/n_s$.

If the load torque is increased, rotor speed falls slightly (and slip increases) so that a larger rotor current is induced, and the necessary motor torque is developed. When the induction motor operates on a standard three-phase supply of constant voltage and frequency, the synchronous speed is fixed, and the shaft speed is always close to the synchronous speed. Traditionally, therefore, the cage-rotor induction motor has been regarded as the premier constant-speed drive, offering ruggedness, reliability, and low cost. However, the advent of modern solid-state power electronics has liberated the induction motor from its historical role as a fixed-speed machine and it now claims a major share of the variable speed drive market. The key to efficient, wide-range speed control is the provision of a variable frequency ac power supply, which permits continuous variation of the synchronous speed of the motor (1,2,3,4,5,6).

Static Frequency Conversion

The variable frequency supply is produced by a converter circuit in which power semiconductor devices function as solid-state switches. The usual converter configuration is the dc link converter shown in block diagram form in Fig. 1. This is a two-stage circuit in which the fixed-frequency 50 Hz or 60 Hz ac supply is first rectified to dc, which is then fed to an *inverter* circuit that generates the variable frequency ac power for the induction motor. A simplified inverter circuit is shown in Fig. 1(a) with the solid-state switches shown as mechanical switches to emphasize the basic on/off action. This mode of operation gives high efficiency because, ideally, the switch has zero loss in both the open and closed positions.

By rapid sequential opening and closing of the six switches in Fig. 1(a), a three-phase ac voltage waveform can be synthesized at the output terminals. The resulting output voltage waveform has a pulsewidth modulated (*PWM*) waveform, as shown in Fig. 1(b). In practical inverter circuits using solid-state switches, high-speed switching is possible, and sophisticated PWM waveforms can be generated with all voltage harmonic components at very high frequencies. The inductive reactance of the motor increases with frequency so that the higher-order harmonic currents are very small, and near-sinusoidal currents flow in the stator windings, setting up an air-gap rotating field, in the usual manner. The fundamental voltage and output frequency of the inverter are adjusted by changing the PWM waveform using the controller of Fig. 1(a), so that speed control of the induction motor is achieved. The voltage level must be altered proportionally with frequency to maintain the correct magnetic conditions in the motor. A reversal of the inverter gating sequence changes the direction of rotation of the motor.

The gating signals from the inverter controller in Fig. 1(a) were traditionally generated using analog circuits, but this function has now been superseded by digital systems. Spectacular advances in microelectronics have provided microcontrollers, signal processors, and application specific integrated circuits (*ASIC*), with dedicated onboard architecture permitting the implementation of computationally intensive drive control strategies, and other tasks such as self-diagnosis, communications, and user configuration. The resulting sophisticated variable- or adjustable-speed drive (*ASD*), is widely used for general purpose applications and in high-accuracy automation systems for industry.

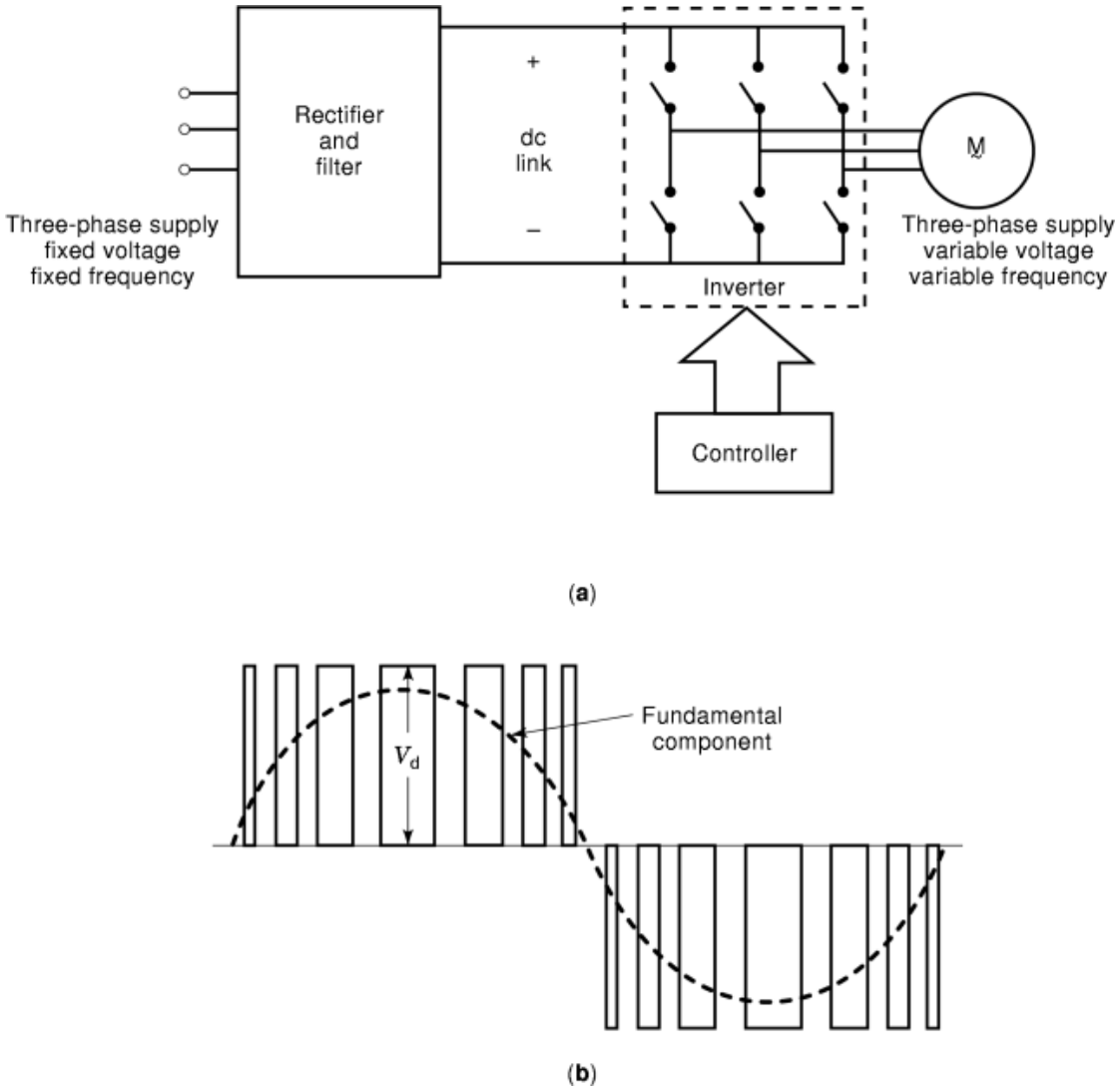

Fig. 1. (a) Functional representation of induction motor drive showing front end rectifier and three-phase inverter with power switches represented as equivalent mechanical switches. (b) Synthesis of the desired variable voltage, variable frequency motor voltage by high-frequency switching of the power switches.

Power Semiconductor Devices

The power semiconductor device is the heart of the power converter. Advances in the cost, size, and performance of modern variable frequency drives can be directly related to the availability of improved power semiconductor switches (7). The principal devices available to the circuit designer are as follows.

Thyristor. The thyristor or silicon controlled rectifier (*SCR*) is a pnpn silicon device with three terminals—anode, cathode, and gate. It latches into the on-state when triggered by a gate current pulse, but turn-off, or *commutation,* can only be achieved by external interruption of anode current. In ac-powered

circuits such as rectifiers and cycloconverters, commutation is accomplished by the natural reversal of the alternating supply voltage, which reduces the thyristor current to zero. However, in dc-powered circuits such as the dc-ac inverter for induction motor control, *forced commutation* is necessary using additional circuitry. These additional components increase inverter size, weight and cost, and consequently, research effort has focused on the development of switching devices with a self-turn-off capability, so that switch turn-off at the gate is possible.

Gate Turn-Off Thyristor (GTO). The GTO is a thyristor-type device that can be turned on and off by positive and negative gate current pulses, respectively. The GTO is available with ratings of several thousand volts and thousands of amperes, and is the predominant device in high-power converters up to several megawatts. However, the turn-off current gain is low and switching losses are high so that the PWM switching frequency is limited to about 1 kHz or 2 kHz.

Power Transistor. The power transistor is a larger version of the normal bipolar junction transistor (*BJT*) with the usual collector, emitter and base terminals. The term bipolar indicates that current flow consists of a movement of positive and negative carriers, that is, holes and electrons. The transistor is switched on and off by the application and removal of forward base current drive. High-current devices have a low current gain but this can be improved in a Darlington power transistor module where an input transistor drives the base of the high-current device.

Power MOSFET. The metal-oxide-semiconductor field effect transistor (*MOSFET*) is a unipolar voltage-controlled device. In the n-channel enhancement mode MOSFET, conduction is by majority carriers (electrons) only, and the absence of positive minority carriers eliminates time delays associated with their removal or recombination. As a result, it is a very fast device and switching losses are negligible up to several hundred kilohertz. Drive power requirements are very small because of the high input impedance, and it is feasible to drive the MOSFET directly from integrated circuit logic. However, the on-state voltage drop increases steeply with voltage rating so that MOSFETs are typically used in low-power converters up to a few kilowatts, with operating voltages not exceeding about 500 V.

Insulated Gate Bipolar Transistor (IGBT). The IGBT is basically a hybrid MOS-gated bipolar junction transistor that combines the best attributes of a MOSFET and a BJT. It has a lower switching loss and a higher switching speed than a BJT and also has the advantage of a high-impedance *MOS* gate drive. The device was commercially introduced in 1983 and has come to dominate the medium power (up to several hundred kilowatts), medium frequency (up to 50 kHz), power converter market.

MOS-Controlled Thyristor (MCT). The MCT is a new device undergoing development. It is a thyristor-like, high-power, high-frequency device with a low on-state voltage and a high-impedance MOS gate. The first commercially available devices were released in 1993 and future devices are expected to challenge the IGBT and GTO.

Power Converters

Inverters can be broadly classified as either voltage-source or current-source inverters (1,2,3,4,5,6). The voltage-fed, or voltage-source inverter (*VSI*), is powered from a stiff, or low-impedance, voltage source and the inverter output voltage is essentially independent of load current. On the other hand, the current-fed, or current-source inverter (*CSI*) is supplied with a controlled current from a high-impedance source so that motor current rather than motor voltage is controlled.

Traditionally, power converters for ac motor drives have used *hard-switching* techniques in which the power semiconductor is highly stressed during the transition between the on and off states when device voltage and current are both large. Snubber circuits are used to alleviate these stresses and divert the switching energy from the device into an auxiliary capacitor or inductor. However, losses in the snubber circuit itself may be significant and consequently, the resonant or soft-switching techniques used in switch-mode power supplies

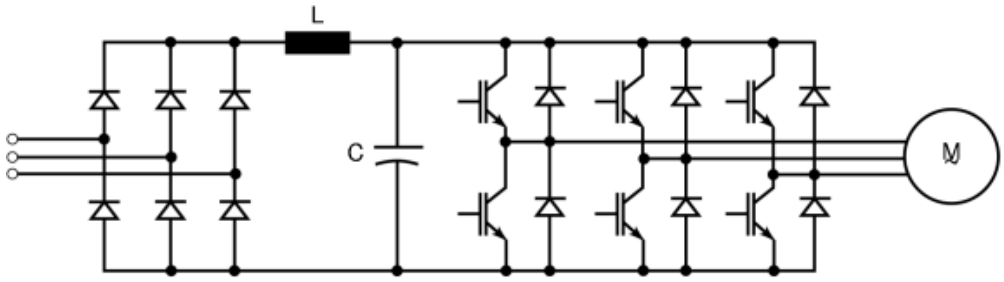

Fig. 2. Practical dc link converter with three-phase diode bridge rectifier front end and dc link filter that provide a stiff dc supply voltage for the inverter stage. The three-phase IGBT-based PWM voltage source inverter is switched to provide the required three-phase variable voltage, variable frequency supply to the induction motor. This power converter topology has become the industry standard induction motor drive.

are now being extended to high-power converters for ac motor drives. Soft-switching converters may employ zero voltage switching (*ZVS*) or zero current switching (*ZCS*) to give snubberless operation with low switching losses and high efficiency.

At lower power levels, semiconductor manufacturers are producing power modules that incorporate the six power switches required for a three-phase bridge voltage source inverter. More sophisticated *intelligent power modules* include gate drivers and protection circuits, offering enhanced reliability and significant reductions in inverter size, weight, and cost.

The PWM Voltage Source Inverter. For variable frequency induction motor drives up to several hundred kilowatts, the standard converter topology is the combination of an uncontrolled diode rectifier and an IGBT-based PWM inverter, as shown in Fig. 2. Note the feedback diodes connected in inverse parallel with the IGBTs to permit the return of energy from reactive or regenerative loads, through the inverter, to the dc link. The IGBTs are switched on and off to develop a three-phase PWM output voltage waveform by adjusting the PWM sequence applied to the inverter. Both output voltage and frequency can be rapidly altered within the inverter circuit, giving the PWM inverter fast transient response, which is essential in high-performance induction motor drives. When controlling the fundamental output voltage, the PWM process inevitably modifies the harmonic content of the output voltage waveform. A proper choice of modulation strategy can minimize these harmonic voltages and the associated harmonic effects in the motor.

Regeneration occurs when the variable speed motor is overhauled by the load, and power is returned to the dc link through the feedback diodes. This regenerated energy cannot be returned to the ac supply network by the diode rectifier circuit in Fig. 2, so a dynamic braking method is usually adopted in which the regenerated power is dissipated in a resistor that is switched across the dc link when the link voltage reaches a certain preset level due to regenerative charging of the filter capacitor.

Modulation Strategies. Early PWM controllers generated inverter firing signals by analog-based comparison of a sine wave modulating signal at the desired output frequency, and a high-frequency triangular carrier wave (1,8). Subsequent digital modulators were based on *regular sampling* in which a sampled version of the sine wave modulating signal facilitated real-time microprocessor-based calculation of the inverter switching points (9). Nowadays, digital PWM modulators are usually based on the principle of *space vector modulation* (*SVM*) in which the state of the inverter is represented by a voltage space vector (10).

In the three-phase inverter of Fig. 3(a), the presence of six power switches implies the existence of eight possible inverter states. For the condition shown, with switches S1, S5, and S6 closed, the voltage of pole A relative to the dc midpoint is $v_A = +V_d/2$, while the pole B and C voltages v_B and v_C, are both $-V_d/2$. This inverter state is represented as [100], where the symbol "1" indicates that pole A is connected to the upper dc rail, and the "0" symbols denote that poles B and C are both connected to the lower rail. Alternatively, the

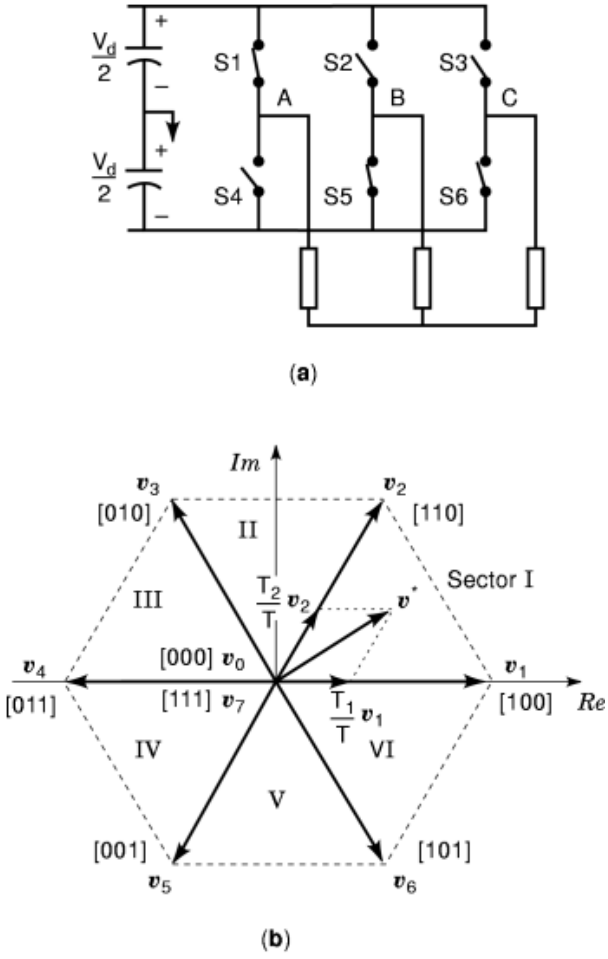

Fig. 3. (a) Representation of one realizable state of a three-phase voltage source inverter. The corresponding voltage space vector is $\boldsymbol{v}_1 = [100]$. (b) Space vector representation of the eight realizable inverter states $\boldsymbol{v}_0$ to $\boldsymbol{v}_7$. Synthesis of desired voltage vector $\boldsymbol{v}*$ by decomposition into realizable inverter states $\boldsymbol{v}_1$ to $\boldsymbol{v}_2$ using the space vector modulation technique.

inverter state may be defined as a complex voltage space vector:

$$\boldsymbol{v} = \frac{2}{3}(v_{\mathrm{A}} + \boldsymbol{\alpha} v_{\mathrm{B}} + \boldsymbol{\alpha}^2 v_{\mathrm{C}}) \qquad (1)$$

where $\alpha = e^{j2\pi/3}$. Thus, for inverter state [100], $\boldsymbol{v} = 2V_{\mathrm{d}}/3$, and lies along the real axis of the complex plane, as denoted by $\boldsymbol{v}_1$ in Fig. 3(b). The voltage space vectors for the other seven states are also represented in Fig. 3(b), which shows six active states with vectors $\boldsymbol{v}_1$ to $\boldsymbol{v}_6$ of equal magnitude, mutually phase displaced by $\pi/3$. In addition, there are two zero states at the origin, $\boldsymbol{v}_0$, [000], and $\boldsymbol{v}_7$, [111], in which all three poles are connected to the same dc rail and the voltage vector has zero magnitude.

For balanced sinusoidal voltages, the required voltage space vector is $\boldsymbol{v} = V_{\mathrm{m}}\, e^{-j\omega t}$, which indicates a vector of constant magnitude, V_{m}, rotating anticlockwise at a uniform angular velocity ω. The three-phase inverter circuit can synthesize this uniformly rotating vector by high-frequency PWM switching between the

realizable discrete voltage vectors, $\boldsymbol{v}_0$ to $\boldsymbol{v}_7$. Suppose, for example, it is required to generate the voltage vector, $\boldsymbol{v}*$, shown in sector I of Fig 3(b). The correct orientation and magnitude of this resultant vector can be achieved by implementing state $\boldsymbol{v}_1$ for time T_1 and state $\boldsymbol{v}_2$ for time T_2, so that

$$\boldsymbol{v}^* = \frac{T_1}{T}\boldsymbol{v}_1 + \frac{T_2}{T}\boldsymbol{v}_2 \qquad (2)$$

where T is the duration of the PWM switching cycle (11). For the remainder of the PWM period, the zero states must be applied for a total time $T_0 = T - T_1 - T_2$. A similar situation, with different active states, arises for operation in any other sector. There are several degrees of freedom for the optimization of space vector modulation, because the discrete voltage vectors can be applied in different sequences and the time T_0 can be partitioned arbitrarily between $\boldsymbol{v}_0$ and $\boldsymbol{v}_7$. The so-called *bus-clamping* techniques minimize the effective inverter switching rate and switching losses by sequentially clamping one of the inverter poles to a dc rail over a portion of the fundamental cycle (12).

Any vector within the hexagon formed by joining the ends of the active vectors in Fig. 3(b) is realizable. Clearly, the largest possible voltage amplitude corresponds to the radius of the largest circle that can be inscribed within the hexagon and is given by $V_d/\sqrt{3}$. Larger fundamental voltages can be realized by abandoning the modulation process and switching the inverter sequentially through the six discrete active states $\boldsymbol{v}_1$ to $\boldsymbol{v}_6$ to complete one cycle. The resulting pole voltages are square waves with an absolute maximum fundamental voltage amplitude of $2V_d/\pi$. The third harmonic and multiples of the third—the so-called triplen harmonic components in the pole voltages cannot appear in the three-phase three-wire load of Fig. 3(a), resulting in a quasi-square line-to-line voltage waveform, and a six-step line-to-neutral voltage. This is the well-known *six-step* mode, usually implemented in PWM drives to give a high-speed field-weakening range of operation with maximum available voltage and variable frequency. By judicious use of the available voltage vectors, it is possible to control smoothly the fundamental output voltage from the $V_d/\sqrt{3}$ limit to that set by six-step operation (10).

Double-Sided PWM Converter. The diode rectifier circuit of Fig. 2 draws a distorted input current, indicating the introduction of significant harmonic currents into the ac network. These harmonic currents introduce supply voltage distortion and degrade network *power quality* for other consumers. Consequently, regulations have been introduced to limit the allowable harmonic currents drawn by power converters. The input diode rectifier stage can be replaced by a PWM inverter operating as a dc-ac converter or *voltage-source reversible rectifier,* as shown in Fig. 4. Using this double-sided PWM converter, the ac currents drawn from the network can be near-sinusoidal and in phase with the ac supply voltage, giving unity power factor operation. This is an expensive method of suppressing harmonic input currents, but the converter is also capable of full regenerative braking for rapid motor deceleration, as the braking energy returned by the motor to the dc link can be fed directly back into the ac network. Thus, the double-converter configuration of Fig. 4 has a bidirectional power flow capability.

The Current-Regulated PWM Inverter. The current-regulated PWM inverter consists of a conventional PWM voltage-source inverter fitted with current control loops. High-performance servo drives, for machine tools and industrial robots, must provide fast dynamic response and smooth rotation down to zero speed. These characteristics necessitate fast closed-loop current control, and the current-regulated PWM inverter is widely used in such drives. Control strategies include simple hysteresis control, ramp comparison control, and predictive control (13,14).

Figure 5 shows one leg of the PWM voltage-source inverter fitted with an analog-based ramp comparison controller. The compensated difference between the reference and actual currents is compared with a fixed-frequency triangular carrier wave. The resulting PWM signal, with a duty cycle proportional to the current error, controls the inverter switching so that the actual motor current closely tracks the reference current.

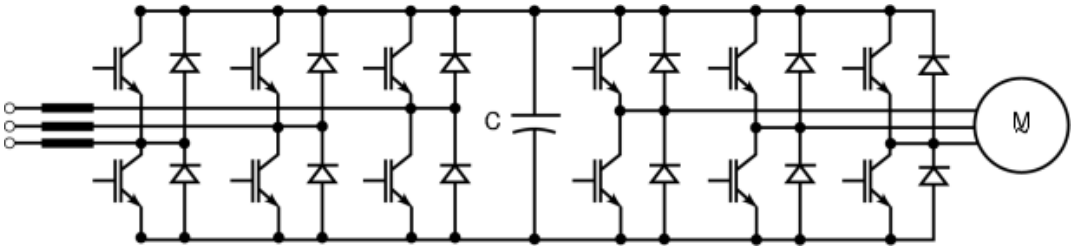

Fig. 4. Double-sided PWM voltage source converter consisting of three-phase IGBT-based front end converter and three-phase IGBT-based voltage source inverter. This configuration allows bidirectional power flow and ac supply current shaping.

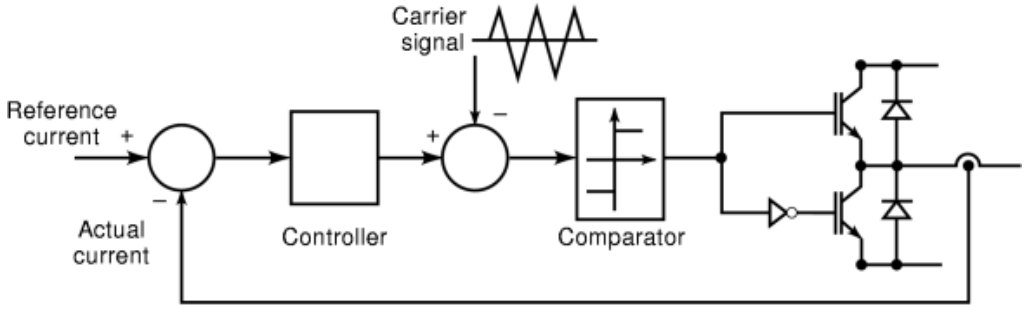

Fig. 5. The current-regulated PWM inverter. Block diagram of PWM current controller for one inverter leg where the compensated current error is compared with a high-frequency carrier waveform in order to generate the switching commands for the two power switches in the leg.

In a three-phase system, there is usually an independent current controller for each inverter phase, but the high-frequency triangular carrier is common to all three phases. In high-performance drives, employing sophisticated microprocessors, the closed-loop control is most often implemented in a synchronous reference frame (15). The resultant steady-state currents assume dc values and improved control robustness is possible.

The Current Source Inverter. The dc link converter can be given the characteristics of a current source by using a front-end phase-controlled thyristor rectifier with a current regulating loop to control its output dc current, I_d (1). Figure 6 shows a typical converter circuit in which the regulated dc link current is fed to a PWM-GTO inverter circuit. The capacitor bank at the motor terminals absorbs the rapid changes in phase current at commutation, and also filters harmonic currents. Note the removal of the shunt capacitor in the dc link and the inverter feedback diodes, which are both characteristically present in a voltage source inverter. Their removal allows a polarity reversal of the link voltage that occurs during regeneration, when energy is returned to the dc link. The phase-controlled converter and its current control loop maintain the demanded current I_d and consequently, the converter delay angle is increased beyond 90° by the control loop, allowing the circuit to function as a phase-controlled inverter returning energy from the dc link to the ac utility network. Thus, the current source inverter drive is inherently capable of regeneration to the input ac power line and has been widely used up to megawatt power levels. Traditionally, conventional thyristors have been used in place of GTOs in the inverter, but forced commutation is then necessary. In the future, large current-source drives will adopt a cascade connection of two GTO-based PWM converters giving bidirectional power flow with sinusoidal input line current shaping and input power factor control. This double-sided current-fed PWM converter is the dual of the voltage-fed system of Fig. 4.

Resonant dc Link Converter. This converter is a modification of the standard voltage-source dc link converter in which a resonant LC circuit is introduced in the dc link (16). By pulsing the resonant circuit

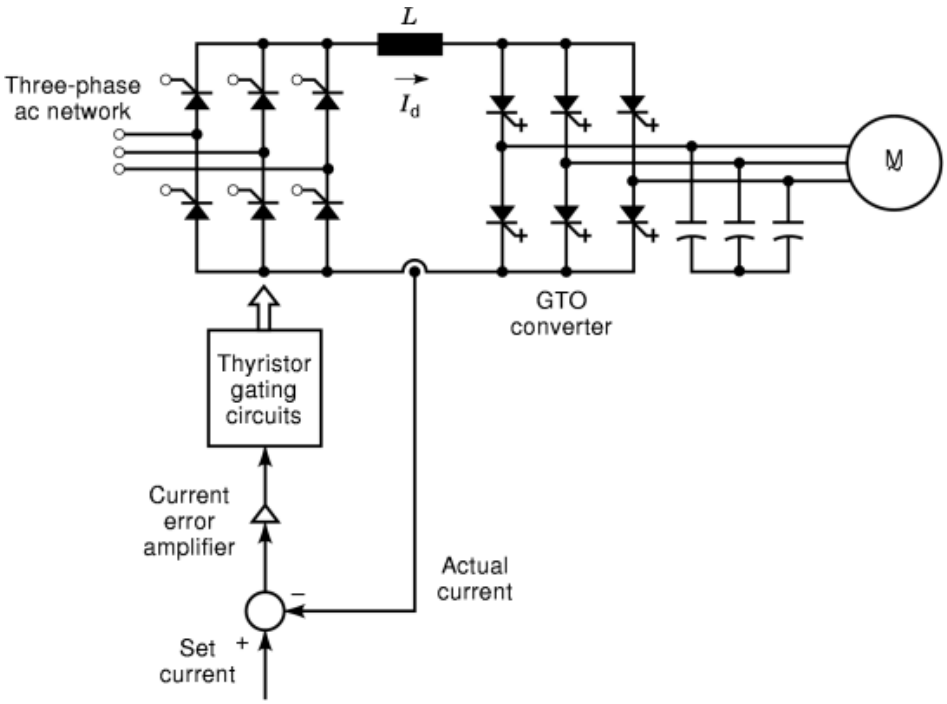

Fig. 6. Dc link converter with phase-controlled thyristor front end converter and closed-loop current control that produce a controlled current I_d in the dc link inductor. The controlled current is switched through appropriate motor phases by the GTO converter.

on and off at high frequency, the inverter input voltage is forced to oscillate between zero and some value that is limited to about 1.5 V_d using an active clamp circuit. During the zero voltage intervals, the inverter devices can be turned on and off, giving all the advantages of zero voltage switching. Each cycle of the low-frequency output voltage waveform must now be synthesized with an integral number of identical dc link voltage pulses. However, if the frequency of the pulsating link voltage is high enough, a good quality output waveform is obtained when an appropriate discrete pulse modulation switching strategy is adopted (17). For inverter ratings in excess of about 300 kVA, the resonant link inductor becomes large and costly, and it is advantageous to use a resonant pole topology in which the dc link voltage is constant and each leg of the inverter has its own auxiliary soft-switching components.

Resonant ac Link Converter. This converter is another modification of the conventional voltage-source dc link converter in which a resonant circuit is introduced between rectifier and inverter so that the link voltage is actually a high-frequency quasi-sinusoidal alternating voltage. Each passage of the link voltage through zero again allows zero voltage switching of the inverter devices. Because the link voltage polarity reverses, the inverter switches are required to be bidirectional and must be realized by connecting two unidirectional switches with reverse blocking capability in inverse parallel. Consequently, twice as many inverter devices are required compared with the resonant dc link topology.

Matrix Converter. The matrix converter is a single-stage ac-ac converter without any intermediate energy storage stage. The three-phase input and output lines are connected by a matrix of nine bidirectional switches so that any output line can be connected to any input line for a controlled time interval (18). The variable frequency output waveform is made up of segments of the fixed-frequency input waveform. This

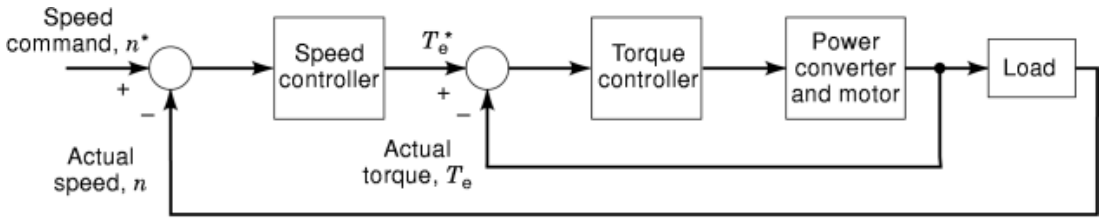

Fig. 7. Closed-loop speed control of a drive system in which cascaded speed and torque controllers are used to give fast accurate four quadrant control of the drive.

concept looks attractive but has proved difficult to implement in a cost-effective manner due to the need for high-performance bidirectional power switches.

Control Techniques for Variable Frequency Drives

The inherent advantages of variable frequency operation of the induction motor cannot be fully realized unless a suitable control technique is employed. Also, the power converter has little excess current capability and, during normal operation, the control strategy must ensure that motor operation is restricted to regions of high torque per ampere, thereby matching the motor and inverter ratings and minimizing system losses. Overload or fault conditions must be handled by sophisticated control rather than overdesign.

Open-loop speed control of an induction motor with a variable frequency supply provides a satisfactory variable speed drive when both the transient performance characteristics are undemanding and the motor operates at steady speeds for long periods. However, closed-loop control is necessary for fast dynamic response and for precise steady-state operation in the presence of load disturbances and supply voltage fluctuations. Figure 7 shows a typical variable speed drive system using a cascaded control structure where the compensated speed error is used to define a torque demand. Inner torque, flux, and current loops may be used to regulate the required electrical characteristics. Unlike the dc motor drive, which has a standard control structure, a wide variety of solutions to the induction motor control problem have emerged to meet different applications and performance requirements. The control schemes of greatest practical importance will now be considered.

Terminal Volts/Hertz Control. This simple form of open-loop control is widely used in general-purpose drives. Such drives are commonly required to have a constant-torque capability over a wide speed range. This characteristic is achieved if the air-gap flux of the motor is maintained constant at all speeds. Operation near the saturation flux density is desirable in order to give maximum utilization of the core material, and it is usual to vary the applied terminal voltage proportionally with frequency to maintain this flux level in the machine. The application of a constant volts/hertz supply gives constant air-gap flux near rated motor frequency, but the stator resistance voltage drop becomes increasingly significant as the frequency is reduced. Consequently, for motoring operation, there is severe underexcitation at low speeds, and an intolerable loss of torque capability. This problem is tackled in general-purpose open-loop drives by implementing a terminal voltage/frequency characteristic in which the voltage is boosted above its frequency-proportional value at low frequencies in order to compensate for the stator resistance voltage drop. However, this preprogrammed voltage/frequency characteristic cannot maintain constant air-gap flux under varying load conditions, because the stator resistance voltage drop is a function of stator current. The disadvantage of this open-loop control scheme is that rotor speed falls as load is increased. Improved speed regulation is possible by the addition of a speed transducer or by implementing either a current-dependent frequency boost or suitable slip regulation (1).

Below base speed, the induction motor has a constant-torque capability. At base speed, the inverter delivers the maximum available output voltage, but the inverter frequency can be increased further, with the same output voltage amplitude, to give a field-weakening region of operation above base speed; as the inverter frequency is increased, the motor has a falling volts/hertz ratio and a falling torque capability. Thus, the complete torque capability curve as a function of speed is very similar to that for a dc machine.

Vector Control. The dc motor is ideal for variable speed applications because the machine construction automatically ensures that the armature magnetomotive force (*mmf*) and main field axes are in quadrature. Field flux is proportional to field current, and torque is proportional to the product of field flux and armature current. Therefore, independent torque and flux control is possible by manipulation of both current components. Similar control of the cage rotor induction motor is more complex because the space angle between the stator and rotor fields varies with load, and rotor current cannot be directly monitored. Vector or field-oriented control permits fast accurate control by decomposing the stator currents into torque and flux components, and transforming the motor to an equivalent separately excited dc machine.

A dynamic model of the induction motor, required for a full understanding of vector control, is written in space vector form in a general reference frame rotating at ω_g as:

$$\begin{aligned}
\boldsymbol{v}_s &= v_{ds} + jv_{qs} = R_s\boldsymbol{i}_s + \frac{d\boldsymbol{\psi}_s}{dt} + j\omega_g\boldsymbol{\psi}_s \\
0 &= R_r i_r + \frac{d\boldsymbol{\psi}_r}{dt} + j(\omega_g - \omega_r)\boldsymbol{\psi}_r \\
\boldsymbol{\psi}_s &= L_s\boldsymbol{i}_s + L_m\boldsymbol{i}_r = L_{ls}\boldsymbol{i}_s + L_m(\boldsymbol{i}_s + \boldsymbol{i}_r) = L_{ls}\boldsymbol{i}_s + \boldsymbol{\psi}_m \\
\boldsymbol{\psi}_r &= L_m\boldsymbol{i}_s + L_r\boldsymbol{i}_r = L_{lr}\boldsymbol{i}_r + L_m(\boldsymbol{i}_s + \boldsymbol{i}_r) = L_{lr}\boldsymbol{i}_r + \boldsymbol{\psi}_m \\
T_e &= \frac{3p}{2}\left(\frac{L_m}{L_r}\right)\boldsymbol{\psi}_r \times \boldsymbol{i}_s
\end{aligned} \tag{3}$$

where $\boldsymbol{i}_s$ and $\boldsymbol{i}_r$ are, respectively, the stator and rotor current space vectors (4). The stator, rotor, and magnetizing flux linkage space vectors are, respectively, ψ_s, ψ_r and ψ_m, and R_s and R_r are the stator and rotor resistances. The stator and rotor self-inductances are L_s and L_r, the stator and rotor leakage inductances are L_{ls} and L_{lr}, and L_m is the magnetizing inductance. The electrical angular rotor frequency is ω_r and the electromagnetic torque is T_e. The real and imaginary components of any space vector are called the direct and quadrature axis components, respectively. In this general reference frame, the stator voltage space vector $\boldsymbol{v}_s$, is obtained from Eq. (1) by applying a vector rotation. Thus, $v_s = ve^{j\theta_g}$, where θ_g is the angular position of the real axis of the rotating reference frame.

Vector control aims to orient the flux-producing component of $\boldsymbol{i}_s$ to some suitable flux vector, under all operating conditions. It is possible to achieve a complete decoupling of the flux- and torque-producing components of the stator current by orientation to the rotor flux vector. Consequently, most research and commercial activity has concentrated on the so-called rotor flux-oriented (*RFO*) control. In the RFO scheme, one component of the stator current is defined in the direction of the rotor flux vector and is used for flux control. The quadrature-current component permits independent torque control. Different implementations are possible, depending on whether or not direct feedback of the amplitude and angular position of the rotor flux vector is available. In the direct RFO (*DRFO*) scheme, the rotor flux is either derived from machine measurements or is accurately estimated from a suitable machine model. Closed-loop torque and flux control is usually implemented. Indirect RFO (*IRFO*) uses the assumed slip relationship of the machine and is generally formulated as a feedforward controller. It is equally possible to orient to more directly accessible quantities such as the stator or air-gap flux vectors. However, the resultant stator flux orientation (*SFO*) and magnetizing flux orientation (*MFO*) schemes are more complex and do not permit completely decoupled torque and flux control.

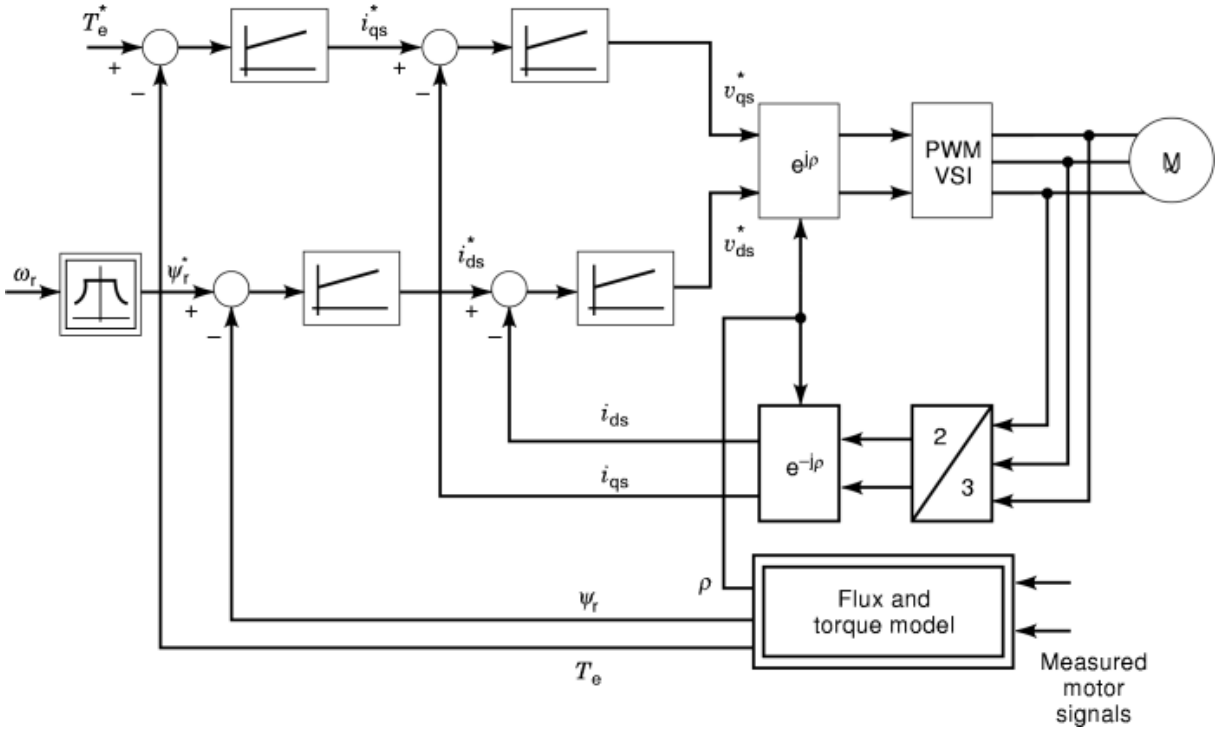

Fig. 8. Structure of direct rotor flux oriented vector control scheme for induction motor in which torque and flux estimates, computed from measured motor signals, are forced to follow the demanded quantities using closed-loop controllers. Inner closed-loop current regulators ensure fast accurate response of the drive system.

Direct Vector Control. The general structure of a DRFO controller is shown in Fig. 8 where torque and flux regulation loops provide the components of the demanded current space vector. Typically, the demanded torque, T^*_e is obtained from a speed control loop, and rated rotor flux is demanded for operation below base speed. In the field-weakening region above base speed, the flux level is reduced because of the finite voltage capability of the inverter. Field orientation is maintained by vector rotations through ρ, the angular position of the rotor flux vector. Closed-loop current control is used to apply the desired stator current vector to the machine. The complete DRFO scheme also requires accurate knowledge of the rotor flux magnitude, ψ_r and electromagnetic torque T_e. Different implementations are possible depending on how the rotor flux magnitude and position are obtained. Torque may be estimated from the flux and measured stator currents using Eq. (3).

The seminal work by Blaschke (19) sensed the air-gap flux using Hall elements for field orientation in an essentially direct MFO scheme. However, from Eq. (3), the rotor flux vector can be derived from the measured magnetizing flux and stator current vectors

$$\boldsymbol{\psi}_r = \psi_r e^{j\rho} = \frac{L_r}{L_m}\boldsymbol{\psi}_m - L_{lr}\boldsymbol{i}_s \qquad (4)$$

so that DRFO is also possible. The use of Hall sensors has been abandoned because of signal distortion due to the rotor slots, and the mechanical and thermal fragility of the sensing elements. Alternatively, it is possible to use special search coils in the motor to measure the rate of change of air-gap flux. However, flux computation

requires pure integration that is difficult at low frequencies due to offset and drift. Consequently, most direct flux measurement schemes have been abandoned in favor of sophisticated estimation techniques.

Two distinct models are used to estimate the rotor flux for DRFO using readily available quantities. The voltage model computes the stator flux, and subsequently the rotor flux, from Eq. (3) with $\omega_g = 0$ as

$$\begin{aligned} \boldsymbol{\psi}_s &= \int (\boldsymbol{v}_s - R_s \boldsymbol{i}_s)\, dt \\ \boldsymbol{\psi}_r &= \frac{L_r}{L_m}(\boldsymbol{\psi}_s - \sigma L_s \boldsymbol{i}_s) \\ \sigma &= 1 - \frac{L_m^2}{L_s L_r} \end{aligned} \tag{5}$$

where σ is the total leakage factor. This method gives good estimates above a few percent of rated frequency, but very low speed performance is degraded due to integrator offset and drift.

An alternative rotor flux estimator, termed the current model, is obtained by eliminating the rotor current from the rotor voltage equation of Eq. (3)

$$\boldsymbol{\psi}_r = \frac{1}{T_r} \int [L_m \boldsymbol{i}_s - (1 - j\omega_r T_r)\boldsymbol{\psi}_r]\, dt \tag{6}$$

where $T_r = L_r/R_r$ is the rotor time constant. This estimator does not require pure integration, and operation down to zero speed is possible. However, a speed-dependent cross-coupling is introduced that may cause numerical instability at high speeds. In addition, the estimator is highly sensitive to variations in the rotor time constant. The flux estimation range can be extended using a closed-loop observer that adds compensated estimation error signals to the voltage model (20). The current model is used to provide the reference for the estimation error calculation and is formulated in the rotor reference frame for increased numerical stability. Correct tuning ensures that the estimator transitions smoothly to the open-loop voltage model as speed increases.

The direct SFO (DSFO) scheme is an alternative vector control strategy for induction motor drives (21). The magnitude and orientation of the stator flux space vector are computed from Eq. (5). The magnitude is used in a closed-loop flux regulator, while the orientation angle is used for vector rotations. The torque may be computed as

$$T_e = \frac{3}{2} p \boldsymbol{\psi}_s \times \boldsymbol{i}_s \tag{7}$$

so that direct torque and flux control is possible without the need for rotor speed or position feedback. Unfortunately, complete decoupling of the torque and flux producing currents is not achieved and a parameter dependent decoupling network must be added. Direct field orientation to the magnetizing flux utilizes a more directly accessible flux quantity and permits easier treatment of saturation effects (22). However, undesirable cross-coupling of the torque producing current is introduced in both the slip and flux equations so that complex parameter sensitive decoupling networks are required.

Indirect Vector Control. Because of the difficulty of good flux estimation at low speeds, indirect vector control gained popularity, because operation to zero speed is possible with the addition of a rotor speed or position transducer (23). Correct field orientation is achieved by computing the desired slip frequency at all operating conditions. Due to the intrinsic decoupling advantages, IRFO control has enjoyed considerable commercial success for high- and medium-performance drives. It is also feasible to structure indirect vector

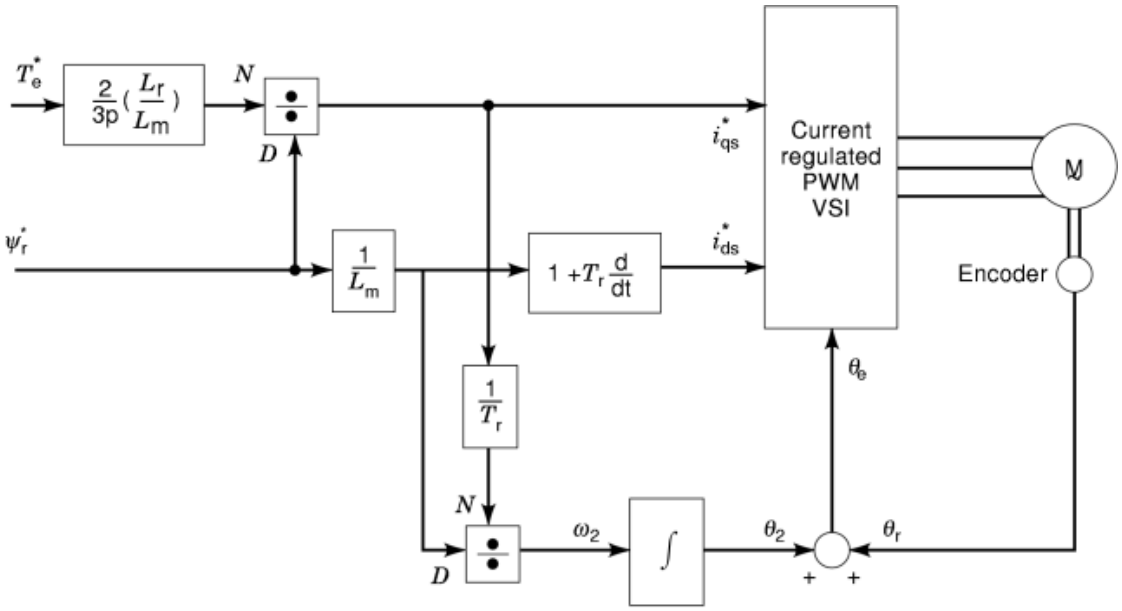

Fig. 9. Structure of indirect rotor flux oriented vector control scheme for induction motor in which the commands for the current regulated PWM VSI are computed from the assumed slip relationship of the machine and estimates of the motor parameters.

controllers that orient to either the stator or magnetizing flux. However, due to an increased computational burden and additional parameter sensitivities, these schemes have received scant attention.

The desired condition for IRFO, $\psi_r = \psi^*_r$, may be used to derive the required stator current components and slip frequency ω_2 in a synchronous reference frame ($\omega_g = \omega_e$). Thus, from Eq. (3)

$$\begin{aligned} i_{qs}^* &= \frac{2}{3p}\left(\frac{L_r}{L_m}\right)\frac{T_e^*}{\psi_r^*} \\ i_{ds}^* &= \frac{1}{L_m}\left(\psi_r^* + T_r\frac{d\psi_r^*}{dt}\right) \\ \omega_2 &= \omega_e - \omega_r = \frac{1}{T_r}\left(\frac{L_m i_{qs}^*}{\psi_r^*}\right) \end{aligned} \tag{8}$$

The IRFO controller is generally formulated as a feedforward structure as shown in Fig. 9. Often, the slip frequency is integrated and added to the measured rotor position θ_r to form the desired synchronous frame rotation angle θ_e used for current control. Because of the feedforward nature of the controller, the IRFO is particularly sensitive to variations in the rotor time constant due to thermal and saturation effects. Such parameter variations can introduce steady-state torque and flux errors, incorrect field orientation, increased motor losses, reduced current regulation capability and undesirable oscillations in the transient torque response (24). Therefore, successful operation of the IRFO scheme is not possible without on-line adaptation that tracks changes in the rotor time constant.

A model reference adaptive system (*MRAS*) can be formulated to track rotor time constant changes by calculating some suitably defined quantity in two different ways, one of which depends intrinsically on the time constant and one of which does not. The error between the two quantities is used to drive the estimation

error to zero. Appropriate reference models include the modified reactive power, the electromagnetic torque, and various voltage terms (25,26,27). However, these methods depend on other motor parameters, suffer performance degradation at low speeds where the stator resistance dominates, and may not operate under light load conditions.

At low speeds and light loads, parameter estimation is possible only by applying suitable perturbations to the motor. One scheme injects a pseudorandom binary sequence (*PRBS*) onto the flux and adjusts the rotor time constant estimate until the crosscorrelation of the flux and measured speed ripple disappears (28). Alternatively, the torque producing current component can be adjusted to avoid torque oscillations, with spectral analysis used for parameter estimation (29). Nowadays, the digital signal processor (*DSP*) can be applied to the on-line parameter estimation using advanced control structures such as the Kalman filter (30). However, expensive floating-point computations are required. The successful on-line estimation of the motor parameters for IRFO without the need for additional transducers or perturbation signals is still the subject of extensive research.

Sensorless Vector Control. In general, rotor speed or position is required for accurate flux estimation in direct vector control or, intrinsically, in the computation of the rotation angle in the indirect schemes. The mechanical sensor adds cost and installation and wiring difficulties to the drive, and reduces the overall ruggedness of the system. Consequently, the development of sensorless vector control schemes has emerged as an important research topic (31). Most strategies for sensorless control rely on an MRAS in which the error between two computations of some suitable quantity is used to force the speed estimate to converge to the correct value (32). However, it is difficult to separate parameter and speed errors in such structures, and very low speed operation is not possible.

An alternative technique for rotor speed and position estimation introduces magnetic saliency in the induction motor by modifying the rotor slot openings so that the rotor leakage inductance becomes position dependent (33). A high-frequency stator voltage is applied, and the corresponding currents are monitored, with the saliency introducing a detectable position dependent modulation. Using a heterodyning process, a derived position error is used as a correction term for a closed-loop speed and position observer. Successful operation to zero speed and under light load is possible. However, a nonstandard induction machine with nonuniform rotor slot construction is required.

Direct Torque Control Strategies. Recently, alternative strategies that directly control the torque and flux without closed-loop current control have emerged. The direct self control (*DSC*) strategy selects one of the six active inverter states by comparing the integrated line-to-line voltages with a reference flux level (34). This causes the stator flux space vector trajectory to move in a direction determined essentially by the particular voltage vector. Application of a zero inverter state causes the flux vector to cease rotation. Thus, the average speed of rotation and the corresponding fundamental period can be controlled by switching between active and zero states. The flux vector follows a hexagonal trajectory such that the stator flux linkage waveform is trapezoidal. However, the deviation of this flux waveform from its fundamental component is so small that machine behavior is not impaired. A comparator-based controller keeps the torque within some defined tolerance band and ensures fast transient response by optimum voltage vector selection. A somewhat different direct torque control (*DTC*) strategy computes the components of the stator flux space vector and electromagnetic torque from measured voltages and currents (35). Again, comparators are used to select the optimum voltage vector that maintains fast torque response and steady-state flux regulation. Unlike the DSC scheme, this strategy constrains the stator flux magnitude to lie within a fixed hysteresis band such that the stator flux vector follows a circular locus and sinusoidal stator flux waveforms are produced. The DTC schemes are particularly applicable to high-power drives where the switching frequency is limited, although commercial implementations are now available for all power ranges.

Advanced Topics in Induction Motor Drives

Selection of Optimum Flux Level. The flux level of the induction machine influences the torque per ampere capability and the overall efficiency of the drive, and should be chosen to meet the required system objectives. In general, high-performance drives require the highest possible torque bandwidths and are operated at constant rated flux up to base speed, so that at light loads the efficiency is suboptimal. Less demanding applications, such as fans and pumps, can improve drive efficiency by reducing the flux level at light load. However, torque response is compromised because rotor flux build up is limited by the rotor time constant.

The efficiency of the induction motor is a complex function of the speed of rotation and the flux and torque levels. Significant improvements in the efficiency can be achieved using a magnetically linear model to predict the optimum operating conditions (36). However, the selection of the optimum flux level is heavily influenced by the nonlinear saturation characteristic. An improved motor model including saturation, stray losses, and skin effect can be used in an iterative calculation of the optimum voltage and frequency for the machine. The computational difficulties can be avoided by measuring the input power to the drive and adaptively reducing the rotor flux until the drive efficiency is maximized. However, this technique requires the addition of extra transducers that may add unacceptable costs to the overall system (3).

Generally, in the field-weakening region, the rotor flux of the machine is reduced at a rate inversely proportional to the speed of rotation, and the drive operates with constant power. This method permits speeds many times base speed to be attained, but optimum torque per ampere is not achieved. Near optimal performance can be obtained if the stator, as opposed to the rotor, flux reference is reduced inversely with speed (3). However, by considering both the voltage and current limits of the inverter, it is possible to achieve maximum torque per ampere performance in the field-weakening region by suitable regulation of the rotor flux level (37).

Self-Commissioning. Self-commissioning is the off-line parameter determination that enables automatic controller gain tuning for optimal dynamic operation of the drive. The electrical parameters are used for tuning of the current controllers and self-commissioning may also include the identification of the mechanical system to tune outer control loops. Ideally, self-commissioning is performed *in situ* so that the normal operating hardware is used and no additional transducers are required. It is normal to use single-phase excitation so that mechanical shaft locking is not required. A series of tests is performed to estimate all relevant motor parameters sequentially. The stator resistance can be determined from a simple dc test. The stator and rotor time constants may be determined by a recursive least squares algorithm following suitable excitation of the machine (38). The nonlinear magnetic characteristic can be obtained by monitoring the current response to fixed voltage steps for different initial currents. It is possible to compensate for the slight inaccuracies inherent in such measurements due to the single-phase excitation by an artificial stretching of the flux axis (39). Additionally, the corrupting influences of the inverter dead time and on-state voltage can be compensated by an initial estimation of their characteristics (40).

Application of Knowledge-Based Controllers. Knowledge-based structures, such as fuzzy logic and artificial neural networks, are being increasingly applied to control and identification problems in induction motor drives (41). Fuzzy logic continues to gain favor due to its ability to provide precise outputs in the presence of imprecise information. Variables no longer assume fixed states as with classical Boolean logic but are allowed to belong to so-called membership functions that span a range of values with varying degrees of probability. Such flexibility allows for increased robustness in the control of complex, multivariable, nonlinear systems such as the induction motor. These techniques have been applied successfully to the speed control, efficiency optimization, and slip gain tuning of variable speed induction motor drives. However, the practical application of fuzzy logic has been limited, because the development tends to be heuristic and lacks a systematic design procedure.

Artificial neural networks (*ANN*) offer a more systematic approach for estimation and control of complex nonlinear systems. With ANN techniques, there is no requirement for a detailed machine model and improved

robustness can be achieved in the presence of system nonlinearities and parameter variations. ANNs attempt to emulate the behavior of the human brain with artificial neurons connected by appropriate synaptic weights. Such structures compute the desired output pattern from an appropriately weighted summation of input patterns. Successful operation requires the training of the network, usually performed off-line, prior to use. Special software is available that significantly reduces the training effort. Once trained, the ANN may be applied to the estimation and control of torque, flux or power in an induction motor drive and it is expected that many other applications will emerge in the next few years (41).

Converter-Motor Interaction. Continuing development in power semiconductor devices has yielded ever higher switching speeds and faster rise times in PWM voltage waveforms, resulting in some undesirable effects in PWM inverter drives.

Acoustic Noise. The switching harmonics in PWM waveforms generate motor flux and current harmonics, which interact to produce high-frequency torque pulsations and irritating acoustic noise. If the PWM switching frequency is fixed, the acoustic noise is characteristically tonal (at discrete frequencies) and may be accentuated by excitation of mechanical resonances in the drive system. The problem is avoided if the switching frequency can be increased to an ultrasonic value (e.g., 20 kHz), but this is not possible at high power levels with slower switching devices. Random PWM techniques have been suggested, in which the inverter switching pattern is randomly varied so as to shift the harmonic power to the continuous spectrum (42).

Motor Insulation Stress. Inverter switching times are now commonly much less than 1 μs, with resulting dv/dt values of 5 kV/μs, or more. Such steep-fronted voltages are propagated along the cables to the motor as traveling waves, according to the laws of transmission-line theory. The surge impedance of the cable is usually appreciably less than that of the motor, causing the incident PWM voltage pulse to be almost doubled in magnitude at the motor terminals (with superimposed high-frequency ringing). These effects become important with long cables and fast rise times, and the resulting overvoltages may damage motor winding insulation (43). The danger is exacerbated by the fact that the steep-fronted voltage pulse is unevenly distributed over the motor winding, with the bulk of the voltage appearing across the end turns. Suggested remedies include reduction of voltage rise time by insertion of series inductors in the motor cables, or modification of motor surge impedance by a resistance-capacitance network at the motor terminals, or the use of double or triple insulated coil wire.

Motor-Bearing Currents. Recent experience also suggests that PWM waveforms with high switching frequencies and fast rise times can cause harmful current flow through motor bearings, leading to material erosion and premature bearing failure. The problem arises from capacitively coupled stator voltages that build up across both motor bearings. These voltages produce intermittent dielectric breakdown currents through the bearing grease with resultant damage to the bearing surfaces. Remedies under review include the use of conductive grease in the bearings, or the fitting of brush devices that ground both stator and rotor. Alternative suggestions involve breaking of the current path by insulating both bearings or by inserting an electrostatic shield between stator and rotor (44).

On-Line Condition Monitoring. The replacement of an induction motor following its failure is both costly and disruptive as it often requires a shutdown of the entire plant. Consequently, much effort has focused on the development of on-line condition monitoring schemes that signal the emergence of potential motor faults. Armed with such knowledge, it is possible to schedule preventative maintenance or replacement during noncritical times. Traditionally, thermal and vibration measurements have been used to detect failures due to broken rotor bars, motor-bearing failures, and mechanical imbalances due to air-gap eccentricities. However, it is possible to use the power of modern digital processors to eliminate the need for such special sensors. Instead, a spectral analysis of the stator currents can be used to detect harmonic components that are characteristic of a variety of failure modes (45).

Electromagnetic Compatibility Issues. The growing proliferation of power electronic equipment has focused attention on the problem of electromagnetic compatibility (*EMC*) between electrical/electronic systems that emit electromagnetic energy and are susceptible to it. Variable frequency drives are sources of emissions, ranging from power frequency harmonics due to the rectifier stage, to the electromagnetic interference (*EMI*)

at lower radio frequencies due to fast switching power semiconductors, and at *UHF* due to microprocessor clocks. Various national and international agencies have produced EMC standards and guidelines (46,47).

Compliance with local power frequency harmonic limits may require the replacement of the traditional diode rectifier input stage with a more sophisticated utility interface circuit (48). Conducted and radiated EMI emissions from conventional hard-switched PWM inverters can be minimized with careful circuit layout, supplemented by snubbers, filters, and shielding. However, the intrinsically low EMI emissions of soft-switched resonant link converters may prove to be their key advantage in an era of global adoption of strict EMC standards.

Communications for Drive Systems. Traditionally, variable speed drives used a ± 10 V analog interface, where the magnitude represented the speed demand and the polarity gave the desired direction of rotation. However, as the need for more sophisticated factory automation systems emerged, more powerful serial fieldbus protocols have been developed. Unfortunately, many of these systems are proprietary and vendor specific so that the user is forced to use equipment from a single source. As a result, various open-architecture, vendor-independent protocols for serial communications have emerged that permit the interconnection of sensors, actuators, drive systems, and programmable logic controllers (*PLC*) from a variety of sources into a single automated process. Examples of such protocols include the Interbus S, Profibus, CAN, SERCOS and MACRO standards whose application in variable speed drive systems is expected to increase (49). These networks allow the transmission of command sequences from a master controller to the drive systems. In addition, measured motor states and characteristics can be transmitted from the drive to the master so that more sophisticated and synchronized control of the entire plant is possible.

Interbus S permits up to 42 drives to be interconnected as a distributed ring with data transmission rates of up to 500 kb/s. The Profibus protocol uses a twisted pair conforming to the RS-485 standard as the physical layer, although fiber optic transmission is also possible. Data rates up to 1.5 Mb/s are possible, although a new 12 Mb/s version has been defined. The CAN standard has gained considerable favor in the automotive industry and permits data rates up to 1 Mb/s, with data transmission only on request. Industrial implementations, such as the Device Net proposed by Allen Bradley, are also available. The SERCOS standard was initiated by a group of German drives manufacturers and users for high-performance systems employing computer numerical control (CNC). The SERCOS standard uses a single fiber optic ring to connect the various drives of the system and data transmission rates of 4 Mb/s are possible. The new MACRO standard permits even faster transmission rates of up to 100 Mb/s and is supported by a variety of American drives manufacturers.

BIBLIOGRAPHY

1. J. M. D. Murphy F. G. Turnbull *Power Electronic Control of AC Motors*, Oxford: Pergamon Press, 1988.
2. W. Leonhard *Control of Electrical Drives.* 2nd ed., Berlin: Springer Verlag, 1996.
3. D. W. Novotny T. A. Lipo *Vector Control and Dynamics of AC Drives*, Oxford: Oxford University Press, 1996.
4. P. Vas *Vector Control of AC Machines*, Oxford: Oxford University Press, 1990.
5. B. K. Bose (ed.) *Power Electronics and Variable Frequency Drives*, New York: IEEE Press, 1996.
6. R. D. Lorenz T. A. Lipo D. W. Novotny Motion control with induction motors, *Proc. IEEE*, **82**: 1215–1240, 1994.
7. B. J. Baliga Power semiconductor devices for variable-frequency drives, *Proc. IEEE*, **82**: 1112–1122, 1994.
8. A. Schönung H. Stemmler Static frequency changers with subharmonic control in conjunction with reversible variable-speed ac drives, *Brown Boveri Rev.*, **51**: 555–577, 1964.
9. S. R. Bowes M. J. Mount Microprocessor control of PWM inverters, *IEE Proc.-B*, **128**: 293–305, 1981.
10. J. Holtz Pulsewidth modulation for electronic power conversion, *Proc. IEEE*, **82**: 1194–1214, 1994.
11. H. W. van der Broeck H. C. Skudelny G. V. Stanke Analysis and realization of a pulsewidth modulator based on voltage space vectors, *IEEE Trans. Ind. Appl.*, **24**: 142–150, 1988.
12. P. G. Handley J. T. Boys Practical real-time PWM modulators: an assessment, *IEE Proc.-B*, **139**: 96–102, 1992.
13. D. M. Brod D. W. Novotny Current control of VSI-PWM inverters, *IEEE Trans. Ind. Appl.*, **IA-21**: 562–570, 1985.

14. J. Holtz S. Stadtfeld A PWM inverter drive system with on-line optimized pulse patterns, *Proc. Eur. Conf. on Power Electron. and Appl.*, **2**: 3.21–3.25, 1985.
15. T. M. Rowan R. J. Kerkman A new synchronous current regulator and an analysis of current regulated PWM inverters, *IEEE Trans. Ind. Appl.*, **IA-22**: 678–690, 1986.
16. D. M. Divan The resonant dc link converter - a new concept in static power conversion, *IEEE Trans. Ind. Appl.*, **25**: 317–325, 1989.
17. G. Venkataramanan D. M. Divan Pulse width modulation with resonant dc link converters, *IEEE Trans. Ind. Appl.*, **29**: 113–120, 1993.
18. L. Gyugyi B. R. Pelly *Static Power Frequency Changers: Theory, Performance and Application*, New York: Wiley, 1976.
19. F. Blaschke The principle of field orientation as applied to the new transvektor closed-loop control system for rotating-field machines, *Siemens Review*, **34**: 217-220, 1972.
20. P. L. Jansen R. D. Lorenz A physically insightful approach to the design and accuracy assessment of flux observers for field oriented induction motor drives, *IEEE Trans. Ind. Appl.*, **30**: 101–110, 1994.
21. X. Xu R. De Doncker D. W. Novotny A stator flux oriented induction machine drive, *IEEE Power Electron. Specialists Conf. (PESC)*, 870–876, 1988.
22. R. De Doncker D. W. Novotny The universal field oriented controller, *IEEE Trans. Ind. Appl.* **30**: 92–100, 1994.
23. K. Hasse *Zur Dynamik drehzahlgeregelter Antriebe mit stromrichtergespeisten Asynchron-Kurzschlussläufermaschinen*, Diss. Tech. Hochschule Darmstadt, 1969.
24. K. B. Nordin D. W. Novotny D. S. Zinger The influence of motor parameter deviations in feedforward field orientation drive systems, *IEEE Trans. Ind. Appl.*, **IA-21**: 1009–1015, 1985.
25. L. J. Garcés Parameter adaption for the speed-controlled static ac drive with a squirrel-cage induction motor, *IEEE Trans. Ind. Appl.*, **IA-16**: 173–178, 1980.
26. R. D. Lorenz D. B. Lawson A simplified approach to continuous on-line tuning of field-oriented induction machine drives, *IEEE Trans. Ind. Appl.*, **26**: 420–424, 1990.
27. T. M. Rowan R. J. Kerkman D. Leggate A simple on-line adaption for indirect field orientation of an induction machine, *IEEE Trans. Ind. Appl.*, **27**: 720–727, 1991.
28. R. Gabriel W. Leonhard C. J. Nordby Field-oriented control of a standard ac motor using microprocessors, *IEEE Trans. Ind. Appl.*, **IA-16**: 186–192, 1980.
29. H. Chai P. P. Acarnley Induction motor parameter estimation algorithm using spectral analysis, *IEE Proc.-B*, **139**: 165–174, 1992.
30. D. J. Atkinson J. W. Finch P. P. Acarnley Estimation of rotor resistance in induction motors, *IEE Proc.-B*, **143**: 87–94, 1996.
31. J. Holz Speed estimation and sensorless control of ac drives, *Proc. IEEE IECON*, 2:649–654, 1993.
32. K. Rajashekara A. Kawamura K. Matsuse (eds.) *Sensorless Control of AC Motor Drives: Speed and Position Sensorless Operation:* New York: IEEE Press, 1996.
33. P. L. Jansen R. D. Lorenz Transducerless position and velocity estimation in induction and salient ac machines, *IEEE Trans. Ind. Appl.* **31**: 240–247, 1995.
34. M. Depenbrock Direct self-control (DSC) of inverter-fed induction machine, *IEEE Trans. Power Electron.*, **3**: 420–429, 1988.
35. I. Takahashi Y. Ohmori High-performance direct torque control of an induction motor, *IEEE Trans. Ind. Appl.*, **25**: 257–264, 1989.
36. J. M. D. Murphy V. B. Honsinger Efficiency optimization of inverter-fed induction motor drives, *Conf. Rec. IEEE Ind. Appl. Soc. Annu. Meeting:* 544–552, 1982.
37. S. H. Kim S. K. Sul Maximum torque control of an induction machine in the field weakening region, *IEEE Trans. Ind. Appl.*, **31**: 787–794, 1995.
38. G. Heinemann W. Leonhard Self-tuning field orientated control of an induction motor drive, *Proc. Int. Power Electron. Conf.*, **1**: 465–472, 1990.
39. N. R. Klaes Parameter identification of an induction machine with regard to dependencies on saturation, *IEEE Trans. Ind. Appl.*, **29**: 1135–1140, 1993.
40. M. Ruff H. Grotstollen Off-line identification of the electrical parameters of an industrial servo drive system, *Conf. Rec. IEEE Ind. Appl. Soc. Annu. Meeting*, **1**: 213-220, 1996.

41. B. K. Bose Expert system, fuzzy logic and neural network applications in power electronics and motion control, *Proc. IEEE*, **82**: 1303–1323, 1994.
42. A. M. Trzynadlowski *et al.* Random pulse width modulation techniques for converter fed drive systems—a review, *IEEE Trans. Ind. Appl.*, **30**: 1166–1175, 1994.
43. A. von Jouanne P. Enjeti W. Gray The effects of long motor leads on PWM inverter fed ac motor drive systems, *IEEE Appl. Power Electron. Conf.* (APEC): 592–597, 1995.
44. J. M. Erdman *et al.* Effect of PWM inverters on ac motor bearing currents and shaft voltages, *IEEE Trans. Ind. Appl.* **32**: 250–259, 1996.
45. R. R. Schoen *et al.* An unsupervised, on-line system for induction motor fault detection using stator current monitoring, *IEEE Trans. Ind. Appl.*, **31**: 1280–1286, 1995.
46. IEEE Std 519-1992, *IEEE Recommended Practices and Requirements for Harmonic Control in Electrical Power Systems*, 1993.
47. IEC 1800-3, *Adjustable speed electrical power drive systems– Part 3: EMC standard, including specific test methods.* International Electrotechnical Commision, 1996.
48. M. Rastogi R. Naik N. Mohan A comparative evaluation of harmonic reduction techniques in three-phase utility interface of power electronic loads, *IEEE Trans. Ind. Appl.*, **30**: 1149–1155, 1994.
49. J. Pisarz E. Hopper A comparative evaluation of industrial field bus systems, *PCIM Europe*, **7** (3): 204-207, 1995.

JOHN M. D. MURPHY
University College Cork
J. F. MOYNIHAN
Analog Devices